

N-Junction Modeling in Perforate Silencers for Internal Combustion Engines

A. Faezian¹, M.R. Modarres Razavi* and A. Onorati²

In this work, boundary conditions of the T -junctions in engine silencers are modeled by the Constant Pressure Model (CPM) and the Pressure Loss Model (PLM). Initially, the mean flow velocity through the ducts is assumed to be zero. Two Benson CPM and Corberan CPM approaches are employed in perforate silencers simulation. For the silencer with more than one perforated pipe, in which N -branch junctions are formed, it is possible to apply the Benson CPM approach. Finally, when the mean flow velocity through the ducts is non-zero, the shortcoming of the CPM model and the ability of the PLM model in describing the T -junctions are shown.

INTRODUCTION

Branch junctions are frequently found in the intake and exhaust systems of multi-cylinder engines, which represent the most complex boundary conditions for wave action models. Most wave action models for intake and exhaust systems are based on the calculation of the flow in the pipes with the one-dimensional assumption. As most frequencies of noise in the exhaust system of engines are less than 3000 Hz [1], the length of waves are long enough and comparable with the length of exhaust system elements, so that 1-D approaches are not far from physical behavior. The flow through branch junctions is always very complex and really multi-dimensional. Therefore, branch junctions must be considered as boundaries between different pipes, where the unsteady calculation should be based on the one-dimensional hypothesis. Onorati et al. [2] applied a hybrid 1D-2D computational approach, in which two models are coupled in the interface boundaries. The 1-D approach is used only for the pipes with constant or gradual changes of the cross section area and smooth bends and the 2-D one is used in complex geometry components such as Y or T junctions. The 2-D model

is based on the Euler equation for compressible non-viscous flow. Although much more information is obtained from the 2-D model than from the 1-D model, its accuracy in predicting the wave motion in the pipes of exhaust systems involving abrupt area changes and T junctions is almost the same. If the main objective is to capture the overall behavior of transmitted and reflected waves, with or without pressure losses, then, simulation of a multi-pipe junction can be based on a 1-D model. Especially in silencer modeling, resorting to 1-D approaches for the simulation of complex silencer geometries with junctions of pipes involved can be beneficial, in terms of simplicity and reduced computational time. A junction of several pipes is called a branch junction. When mass accumulation within the junction is negligible, the conservation laws can be applied without considering any sink or source terms. Flow through a branch junction can be modeled by the use of empirical correlations or by the use of simplified equations, which assume some kind of theoretical behavior of the flow [3]. The modeling of such junctions with one-dimensional simulation is possible and has enough accuracy if some modifications, such as length corrections, are applied on the ends of the pipes. Length correction may be added to the length of the duct adjoining the discontinuity to represent wave reflection and transmission at the boundaries [4,5].

William-Louis et al. [6] described a model based on the method of characteristics for the calculation of pressure wave propagation through a junction. Their method is valid for subsonic flow, taking the

1. Khorasan Science and Technology Park, Technologic Research Institute, P.O. Box 91735-139, Mashad, I.R. Iran.

*. Corresponding Author, Department of Mechanical Engineering, Ferdowsi University of Mashad, P.O. Box 91775-1111, I.R. Iran.

2. Department of Energetics, Politecnico di Milano, Campus Bovisa, Via La Masa 34, 20158 Milano, Italy.

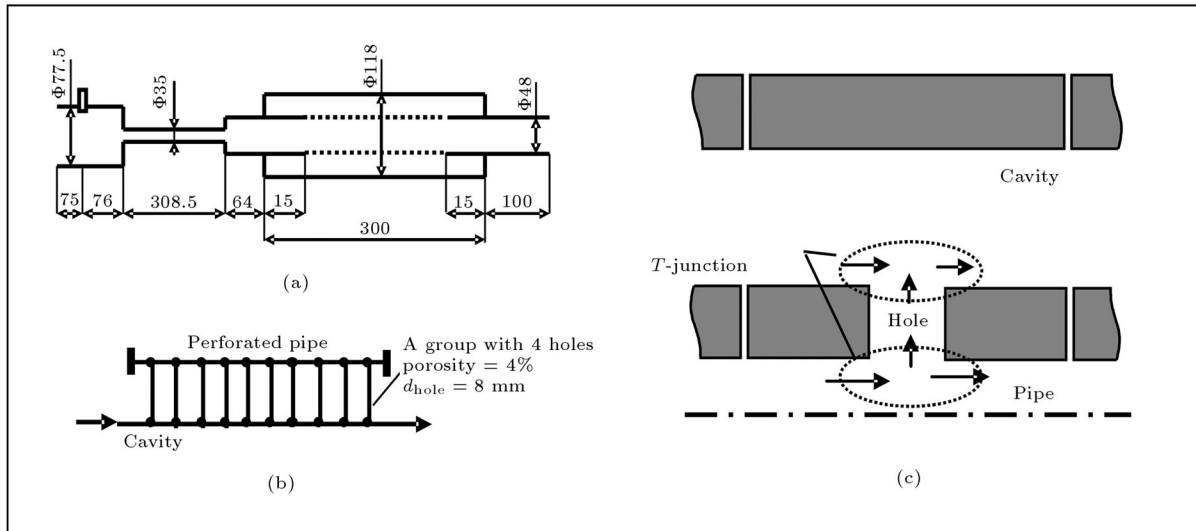


Figure 1. The perforate silencer: (a) Schematic of the system; (b) Acoustically equivalent duct-system; (c) A magnified piece of silencer in which the hole-cavity and hole-pipe connections by means of T -junction is shown.

fluid compressibility and pressure losses into account, according to the type of junction. They used the branch superposition method, which decomposes an N -branch junction into a two-branch junction. In their method, the elementary two-branch junctions are modeled separately. Each elementary junction is formed by an inlet and an outlet branch and other branches are considered as a sink (for the outlet) or a source (for the inlet) of mass and stagnation enthalpy.

There are two ways for dealing with the multi-pipe junctions: The constant pressure and the pressure loss approaches [4]. The simplest method of dealing with a multi-pipe junction is to assume that the static pressure at all of the pipe ends comprising the junction is uniform. This assumption is based on the observations of List and Reyl [7], who showed that for small wave propagation, the pressure drop across a junction is negligible. There are some Constant Pressure Model (CPM) approaches, such as the Benson CPM [7] and the Corberan CPM [7], which can be applied to N -junctions. Another approach, which can be applied to N -branch junctions, is the pressure loss model (PLM). The Benson PLM model [7] is based on an empirical form of the momentum equation incorporating experimental loss coefficients, which are obtained from steady flow tests. The coefficients were only obtained for 90° bends and T -junctions and the calculation procedure was limited to junctions of three pipes. The results of unsteady flow tests showed that the momentum model is superior to the constant pressure models. A similar technique, but with a generalized form of the momentum equation, was used by Bingham and Blair [8]. Junctions in the engine manifolds are classified as supplier and collector types.

In the generalized PLM method by Bingham and Blair, the loss coefficients are based on experimental results and are related to the angles between pipes. Bassett et al. [9] presented a technique for estimating the pressure loss coefficients for junctions instead of using experimental data for the steady-flow condition.

Morel et al. [10] split the perforate silencers into subdivided volumes and Y -junctions, where more than two ducts are connected together. Onorati [4,5] modeled perforate silencers by resorting to acoustically equivalent duct-systems. He considered perforate holes as short ducts and used the Corberan CPM approach to represent T -junctions of the duct-system. Figures 1a and 1b show the schematic and the acoustically equivalent of a perforate silencer, respectively. The short ducts connect the cavity and the perforated pipe together, forming the T -junctions, as shown in Figure 1c.

In this work, the two Benson's CPM, Corberan's CPM and, also, Benson's PLM approaches are applied to N -junctions of perforates. The performances of these approaches are studied and compared with each other. The calculation of the wave motion in the duct-systems is performed by a one-dimensional non-linear model using the two-step Lax-Wendroff method and the MacCormack predictor-corrector method with second order accuracy, resorting to flux limiting techniques (FCT, TVD algorithms) to get oscillation-free solutions [7].

CONSTANT PRESSURE MODEL FOR PIPE JUNCTIONS

When the CPM models are applied to multi-pipe junctions, the characteristics of such junctions are

defined by geometric cross section areas and, therefore, it is not necessary to carry out flow measurements on the junctions, as is required with the pressure loss model. This is a great advantage, because flow tests are both time consuming and expensive. A great advantage of the constant pressure junction theory is that it is not limited by the number of pipes that may be joined [7].

Benson's CPM Approach to the N -Junction

Benson, in his model, assumed that the volume of the junction is small compared with the volume of the pipes. To obtain the entropy levels of the pipe ends at the junction, the following assumptions were made by Benson et al. [7].

For pipe ends in which the flow is towards the junction (gas velocity U^* positive), the entropy level is not changed (i.e. $(A_{Aj})_{j=NJ}$ equals previous values of A_{Aj}).

For pipe ends in which the flow is away from the junction (gas velocity U^* negative), the entropy level at the pipe is the weighted mean of entropy levels of the joining flows.

As shown in Figure 2, N pipes are joined in an N -junction. The joining flows are numbered from 1 to NJ and separating flows from $NJ + 1$ to $NJ + NS = N$. Benson ignored the N -junction volume (quasi-steady approach). As a result, there are $3N$ unknowns, at any end (pressure, temperature and velocity). Both continuity and energy equations govern the junction. There are N relations that describe the incident Riemann variables of all the pipes and NJ relations of joining flows entropy level. The sum of these equations is $N + NJ + 2$, so that $N + NS - 2$ equations must be found. In addition, there can be obtained $N - 1$ independent equations from the constant pressure assumption in the N -junction (Equation 1). If there are $NS - 1$ other equations, they are enough for solving the N -junction. Benson assumed that the entropy levels of all separating flows are the same and equal to the average

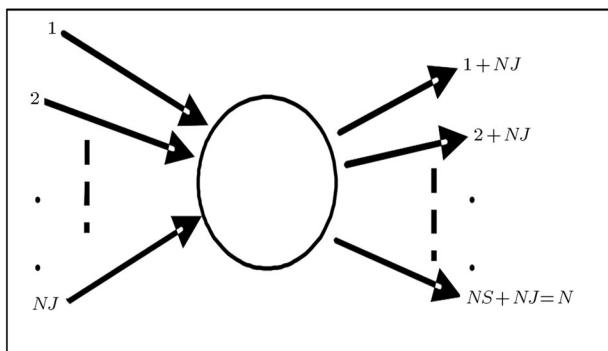


Figure 2. NJ joining flows (towards the junction) and NS separating flows (away from the junction).

entropy level of the joining flows [3]:

$$A_j^* = \frac{\sum_1^N \left(\frac{\lambda_{in_j}^* F_j}{A_{Aj}} \right)}{\sum_1^N \left(\frac{F_j}{A_{Aj}} \right)} = \left(\frac{p_j}{p_{ref}} \right)^{\frac{k-1}{2k}}, \quad (1)$$

$$A_{Aj} = \frac{\sum_1^{NJ} (U_j^* F_j A_{Aj})}{\sum_1^{NJ} (U_j^* F_j)} \quad j = (NJ + 1) \text{ to } N. \quad (2)$$

The relationship between entropy level and starred variables are derived in Equation A1 of the Appendix. For perforate junctions, the summations involved in Equation 1, concerning all the ducts meeting at the junction, can be reduced to the sum of three terms, related to the three pipe ends entering the T junction. In fact, the numerous short ducts standing for the holes in each T junction can be well represented by a single hole-duct with the real geometrical dimensions, since the holes are identical and experience the same fluid dynamic and acoustic behavior. By introducing the number of perforate holes per group n_{holes} , the corresponding term in the following equation is derived:

$$A_j^* = \frac{\frac{\lambda_{in_1}^* F_1}{A_{A_1}} + \frac{\lambda_{in_2}^* F_2}{A_{A_2}} + n_{holes} \frac{\lambda_{in_3}^* F_3}{A_{A_3}}}{\frac{F_1}{A_{A_1}} + \frac{F_2}{A_{A_2}} + n_{holes} \frac{F_3}{A_{A_3}}} = \left(\frac{p_j}{p_{ref}} \right)^{\frac{k-1}{2k}}, \quad (3)$$

subscripts $j = 1$ to 3 refer to the pipe ends; subscripts 1 and 2 indicate left and right ducts belonging to the perforate pipe or to the cavity (Figure 1), whereas subscript 3 indicates the hole-duct representing the group of n holes (hence, F_3 is the single hole area).

Similarly, the dimensionless continuity equation at the junction can be written as:

$$\frac{(A_1^*)^{\frac{2}{k-1}} U_1^* F_1}{A_{A_1}} + \frac{(A_2^*)^{\frac{2}{k-1}} U_2^* F_2}{A_{A_2}} + n_{holes} \frac{(A_3^*)^{\frac{2}{k-1}} U_3^* F_3}{A_{A_3}} = 0. \quad (4)$$

A silencer with two perforated pipes in the cavity has been simulated in the same way, as a silencer with one. Figures 3a and 3b show the schematic and the acoustic equivalent of a two pass perforate silencer, respectively. One of the 4-junctions connecting the cavity with two perforated pipes is magnified, as shown in Figure 3c. In this case, there is more than one group of holes connected to the T junction; hence, each group of holes can be represented by a single hole-duct, introducing the corresponding number of holes, n , in the boundary equations. For example, the continuity equation in this

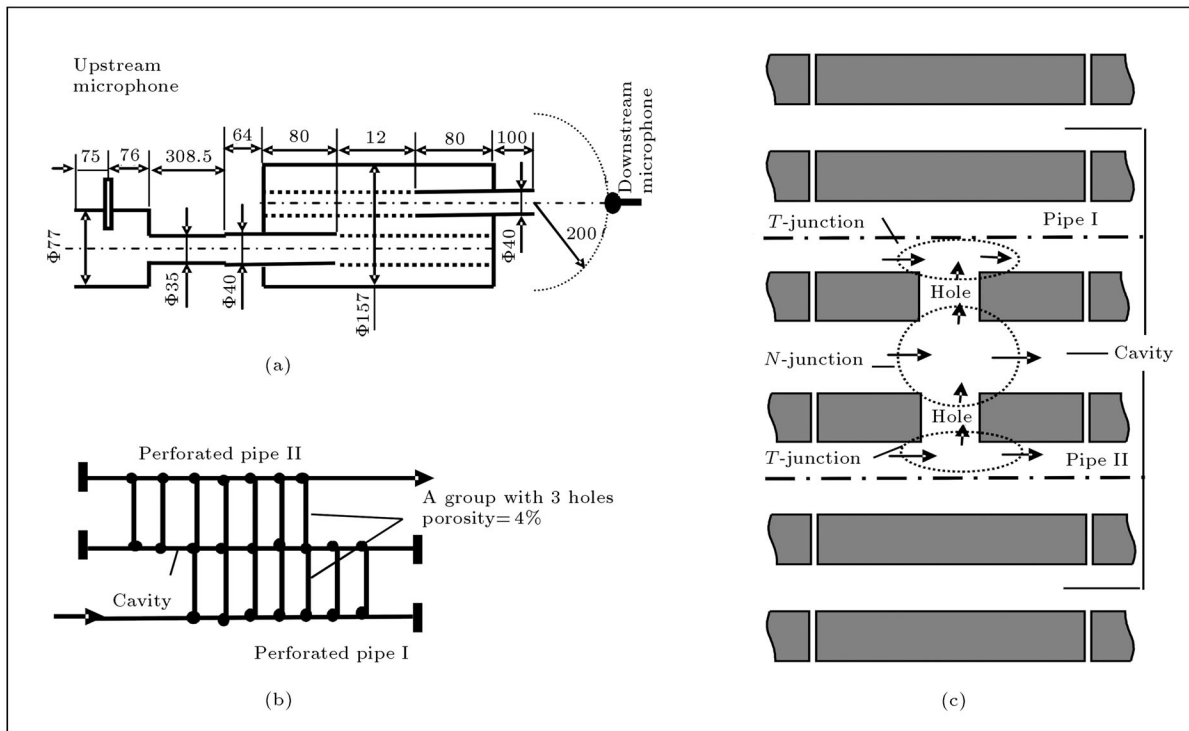


Figure 3. Two pass perforate silencer: (a) Schematic of the system; (b) Acoustically equivalent duct-system; (c) A magnified piece of silencer in which the hole-cavity and hole-pipe connections by means of *T*-junctions and *N*-junctions are shown.

case becomes:

$$\begin{aligned}
 & \frac{(A_1^*)^{k-1}}{A_{A_1}} U_1^* F_1 + \frac{(A_2^*)^{k-1}}{A_{A_2}} U_2^* F_2 \\
 & + \left(n_{\text{holes1}} \frac{(A_3^*)^{k-1}}{A_{A_3}} U_3^* F_3 \right)_{\text{1st group of holes}} \\
 & + \left(n_{\text{holes2}} \frac{(A_4^*)^{k-1}}{A_{A_4}} U_4^* F_4 \right)_{\text{2nd group of holes}} \\
 & = 0.
 \end{aligned} \tag{5}$$

Corberan's CPM Approach to the *N*-Junction

Corberan adopted Benson's assumption for the entropy level of separating flows and modified it in this way: although the entropy levels of all the separating flows are the same, this is not necessarily equal to the average entropy level of the joining flows (Equation 6). He called it the equal entropy approach. In a different approach, he assumed that the total enthalpies of all separating flows are equal (Equation 7). It means that the joining flows have enough time to mix completely. He called it the equal total enthalpy approach. He showed that the equal entropy and the equal total enthalpy approaches will be the same for low mean

velocity and temperature [3,7]:

$$A_{A_i} = A_{A_j}, \quad i \neq j \in \{(NJ + 1) \text{ to } N\}, \tag{6}$$

$$A_{A_i}^2 \left(A_i^{*2} + \frac{k-1}{2} U_i^{*2} \right) = A_{A_j}^2 \left(A_j^{*2} + \frac{k-1}{2} U_j^{*2} \right),$$

$$i \neq j \in \{(NJ + 1) \text{ to } N\}. \tag{7}$$

BENSON PLM APPROACH TO THE *T*-JUNCTION

The CPM model is a simple and useful approach for dealing with junctions in which the velocities and pressure losses are low, but it has shortcomings when applied to the simulation of the behavior of typical engine manifold junctions. Benson et al. developed a Pressure Loss Model (PLM) to consider pressure losses in the *N*-branch junctions. Benson PLM approach is limited to the *T*-junctions and is based on two assumptions [11,7]:

- The flow is one-dimensional across any section at the end of a pipe in which the flow is towards the junction;
- The pressures are equal in the two pipes in which the flow is towards the junction.

The areas of the three cross-sections of the T -junction are considered equal, since the only experimental loss coefficients for this case are available. As shown in Figure 1, the holes (short ducts) are connected to the perforated pipe on one side and to the cavity from the other side. There are six cases which can occur in junction flows. T -junction flows are divided into three joining and three separating flow cases [7]. The patterns and cases of these flows are shown in Figure 4. The quasi-momentum equations are applied to describe pressure losses between sections of the T -junctions originated by pipe-hole and hole-cavity connections. These equations could be derived for all types of flow (all the flow cases and the corresponding quasi-momentum equations are explained in detail in [1]). The following Equations are an example for the flow case shown in Figure 4b:

$$p_1 - p_2 = C_1(\rho_2 u_2^2 - \rho_1 u_1^2),$$

$$p_1 - p_3 = C_2 \rho_3 u_3^2. \tag{8}$$

The pressure difference equations can be combined with the continuity equation and the steady flow equations [11]. There are two forms of the energy equation, one for the joining flows and one for the separating flows. The energy equation for joining flows becomes:

$$\sum_{j=1}^3 (m h_o)_j = \sum_{j=1}^3 (\rho u F h_o)_j = 0. \tag{9}$$

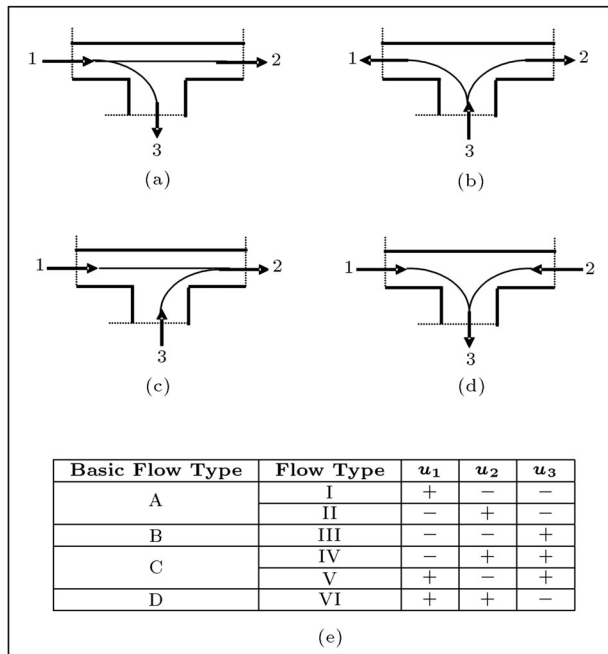


Figure 4. The T junction flow patterns; (a) and (b) Separating flows; (c) and (d) Joining flows; (e) Table of flow cases.

The energy equation can be derived in the following form by using the starred variables A^* and U^* :

$$\sum_{j=1}^3 \left\{ A_{Aj} (A_j^*)^{\frac{2}{k-1}} U_j^* \left(A^{*2} + \frac{k-1}{2} U^{*2} \right) F_j \right\} = 0. \tag{10}$$

For separating flows, the stagnation enthalpy is constant along a streamline of the junction as:

$$h_{o1} = h_{o2} = h_{o3}. \tag{11}$$

It can be derived in the following form by using the starred variables A^* and U^* as:

$$A_{A1}^2 \left(A_1^{*2} + \frac{k-1}{2} U_1^{*2} \right) = A_{A2}^2 \left(A_2^{*2} + \frac{k-1}{2} U_2^{*2} \right)$$

$$= A_{A3}^2 \left(A_3^{*2} + \frac{k-1}{2} U_3^{*2} \right). \tag{12}$$

It is necessary to relate the pressure difference terms to the starred variables. The resulting expression for all the flow types is:

$$\left(\frac{A_j^*}{A_1^*} \right)^{\frac{2k}{k-1}} + G_1 \left(\frac{A_j^*}{A_1^*} \right)^{\frac{2}{k-1}} - G_2 = 0 \quad j = 2, 3. \tag{13}$$

Functions G_1 and G_2 for the different flow types are reported in Table A2 of the Appendix. Also, in this boundary condition, the short ducts representing the holes in each T junction can be treated as a single hole-duct with the real geometrical dimensions, by introducing the number of holes per group, n_{holes} , in the continuity and energy equations.

EXPERIMENTAL APPARATUS

A simple experimental apparatus [5] has been employed in a semi-anechoic room to measure the tailpipe noise and the attenuation curve of several silencers. The schematic of the experimental rig is shown in Figure 5. This has been used with acoustic excitation provided by a loudspeaker and zero mean flow or with high amplitude excitation and strong mean flow provided by an engine. In this study, only the zero mean flow cases were considered. In the case of acoustic excitation, the loudspeaker is insulated in a sound-proof box and radiates white noise (generated by the spectrum analyzer), which is used to excite the wave motion in the silencer system. Two microphones are used with acoustic excitation. The first microphone measures the pressure within the pipe (the upstream pressure), while the second microphone records the pressure field at a distance l from the tailpipe end (the downstream pressure). The signals from the two microphones reach the spectrum analyzer via two phonometers. The downstream microphone is placed

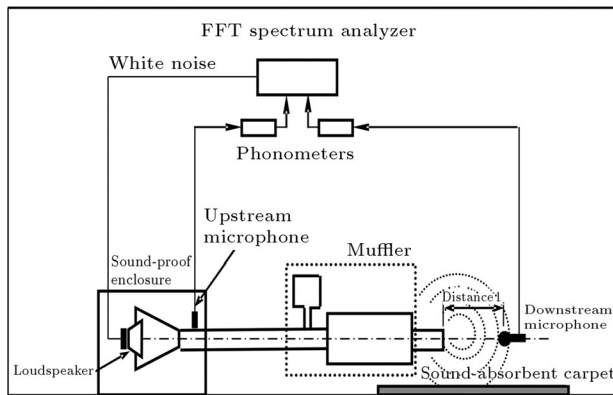


Figure 5. Schematic of the experimental rig adopted for the acoustic excitation of silencing systems.

at a distance of 0.5 m from the open end and at an angle of 45° to the pipe axis. A sound-absorbent carpet is placed under the open termination to reduce the influence of ground reflection and achieve a quasi-spherical radiation.

The spectrum analyzer performs an FFT analysis of the two signals and evaluates the transfer function (i.e. the attenuation curve) in the frequency domain by taking the difference between the upstream and downstream sound pressure level spectra in dB. The transfer function of the acoustic filter can be measured by means of two microphones (the first upstream of the silencer, the second at a certain distance from the open termination). Transfer function and transmission loss of a system are introduced in Equation A3 of the Appendix.

RESULTS AND DISCUSSIONS

In the single-pass perforated tube silencer, almost the same results are obtained from the two Benson and Corberan CPM approaches, so that it is almost impossible to recognize any difference between the results. Comparison of the predicted and the experimental results for zero mean flow of a perforate silencer with a single perforated pipe is shown in Figure 6. Onorati [5] applied the Corberan approach on perforate silencer modeling. In this work, it was found that when the Corberan approach is applied to the N -junctions of silencers with more than one perforated pipe (Figure 3), the calculation can be unstable. By reviewing the formulations of the two approaches, it is observed that in the Benson CPM procedure (Equation 2), the entropy levels of separating flows are the same and equal to the average entropy level of joining flows. This procedure controls the oscillations of entropy levels and does not allow them to overshoot. Therefore, the N -junctions of perforate silencers with two perforated pipes (Figure 3) are modeled by the Benson CPM approach. The predicted results are

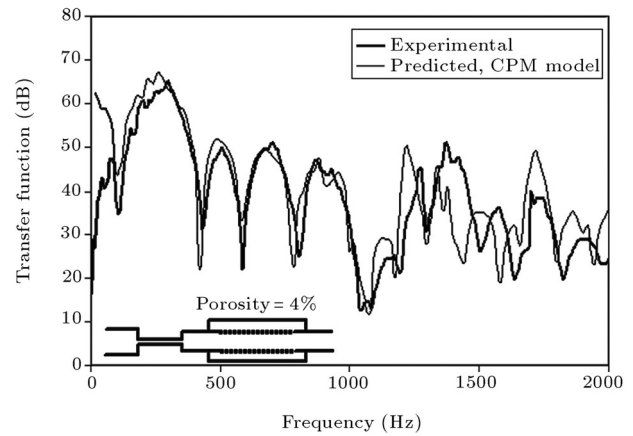


Figure 6. Comparison between the predicted results of perforate silencer (Figure 1), achieved by the Benson and Corberan CPM approaches and the experimental data.

compared with experimental results for zero mean flow in Figure 7. It can be seen from Figures 6 and 7 that the predicted results follow the experimental results closely, especially for the resonant frequencies. Some oscillations of the predicted results may be related to the kind of upstream excitation, which is white-noise. In Figures 6 and 7 the transfer function is calculated based on the upstream excitation source to be white-noise.

Also, the Benson PLM approach has been applied to the N -junctions for the case of zero mean flow. The mean flow is explained in Equation A4 of the Appendix. A simple configuration with a single-pass perforated tube, closed in the middle, has been considered (Figures 8a and 8b), as reported in [12]. Figure 8c shows numerical results, predicted by CPM model and the predicted PLM model results. The PLM approach is imposed in three ways:

1. For all flow patterns of Figure 4 (it is indicated in Figure 8c by a middle wide line);

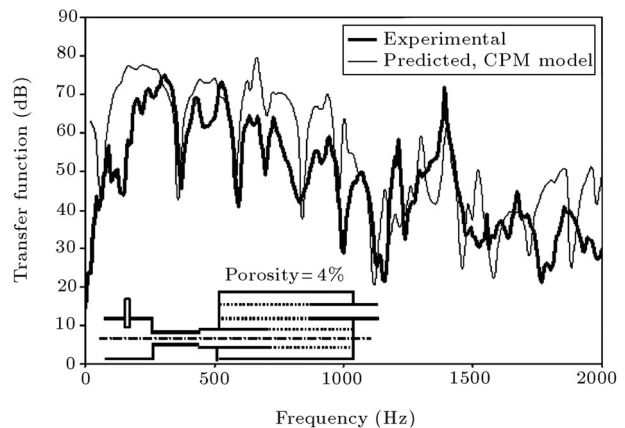


Figure 7. Comparison between the predicted results of two pass perforate silencer (Figure 3), achieved by the Benson CPM approach and the experimental data.

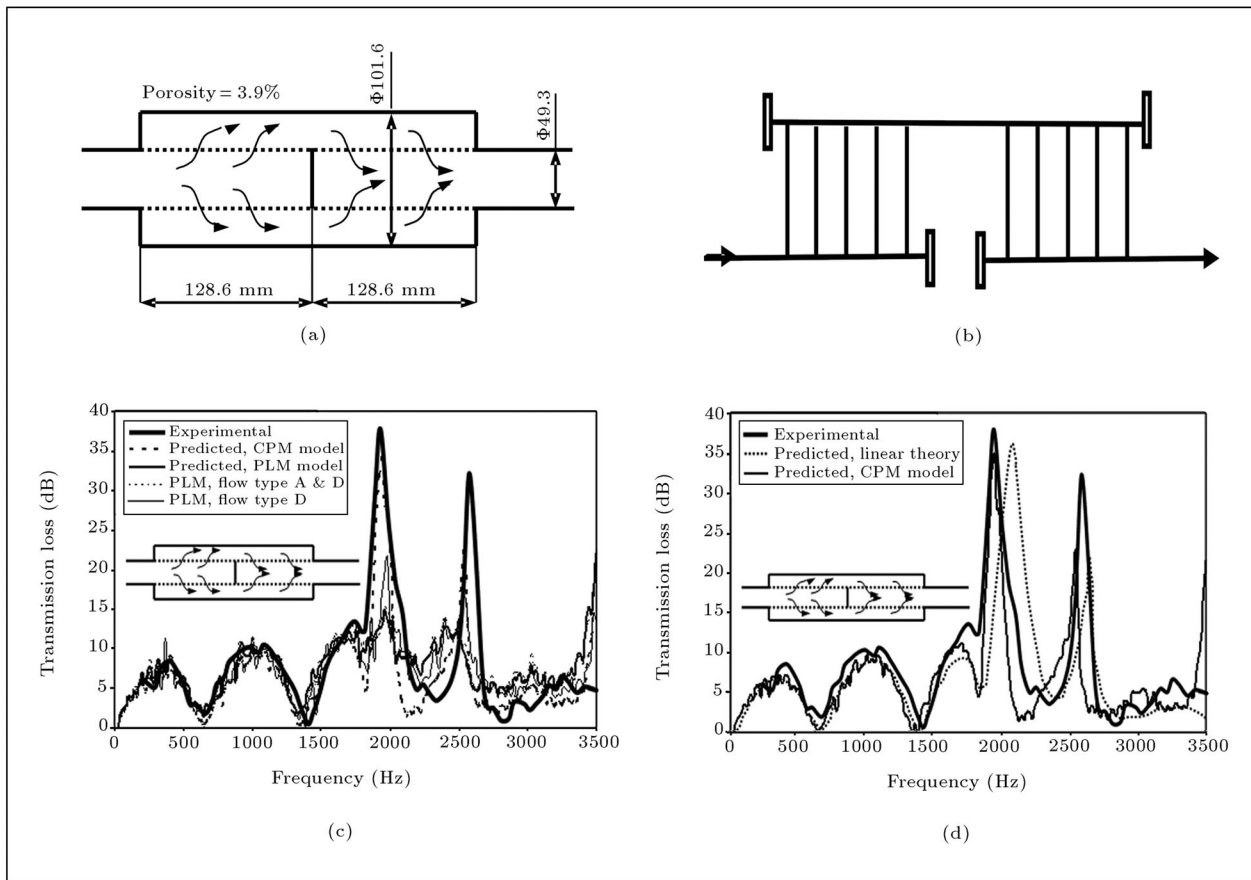


Figure 8. Single pass perforate tube silencer closed in the middle: (a) Schematic of the system; (b) Acoustically equivalent duct-system; (c) Case of zero mean flow, comparison between the predicted results achieved by the CPM and the PLM approaches and the experimental data taken from [12] (d) Comparison between the predicted results by the CPM model and the theoretical linear approaches and the experimental data taken from [12].

- For (a) and (d) flow patterns of Figure 4 (it is indicated in Figure 8c by a dash line);
- For (d) flow pattern of Figure 4 (it is indicated in Figure 8c by a narrow line).

The CPM results are more accurate than the PLM ones. The results of the third PLM approach are not as good as the CPM approach but are better than the first and second PLM approach. Moreover, in Figure 8c, the experimental resonance at about 2600 Hz is not well captured by the CPM model. In Figure 8d, these numerical results are compared with theoretical linear results. It can be seen that resonance frequencies and amplitudes of transmission loss, which are predicted by this numerical method, are better than a theoretical linear one. An end correction length is added to the length of the duct to overcome the shortcomings of the 1-D model on the geometrical discontinuities. This correction length depends on the geometry of the discontinuity and on the frequency of the wave. Since the white-noise excitation is used in upstream of the silencer, a fixed correction length must be used for

all frequencies. Thus, the adopted correction length will provide less accuracy for high frequencies. The experimental results in the low frequency band (less than 250 Hz) are not reliable for all experimental measurements.

For non-zero mean flow (Figure 9), the pressure losses in the N -junction and in sudden area changes are considerable. In this case, the Benson CPM and PLM approaches have been applied to the T -junctions of perforate silencers. In the PLM approach, the pressure losses in the N -junction are imposed directly, whereas in the CPM approach they are ignored, although their effects are considered by a friction coefficient equal to 0.08 along the short ducts (holes) connected to the N -branch junctions. When the PLM approach is used, due to the lack of experimental data for the case of non-equal cross-section areas of the connecting ducts to the T -junction, the pressure loss coefficients are based on the experimental data for equal cross-section areas. The friction coefficient of the holes (short ducts) is considered to be 0.08 (greater than the typical value of 0.005). The higher value of the

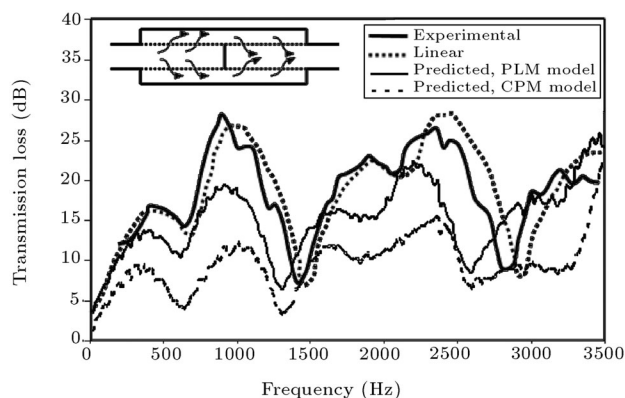


Figure 9. Comparison between the numerical predicted results of silencer shown in Figure 8 (non-zero mean flow case, Mach number = 0.05) achieved by the CPM and PLM approaches, theoretical linear predicted results [12] and the experimental data taken from [12].

short duct friction coefficient somehow compensates for the lower value of cross-section area. The results for the silencer of Figure 8a are shown in Figure 9. The Mach number (calculated on the basis of the mean velocity) is about 0.05 in this case. Since the perforated pipe in the silencer is closed in the middle, as shown in Figure 8, the whole gas flow has to pass through the holes. This condition is more suitable for evaluating the ability of the PLM model. There is a good agreement over the frequency range of 0-2000 Hz between the predicted results and the measured data reported in [12] for this case, as shown in Figure 9. It should be noted that the theoretical linear results by Sullivan, J.W. [12] are closer to the experimental results. In Figures 8 and 9 the transmission loss is calculated based on the upstream excitation source to be white-noise.

CONCLUSIONS

The conclusions of this research work are:

- For the single-pass perforated tube silencer and the case of zero mean flow, the Benson CPM and the Corberan approaches provide the same results;
- The Benson CPM approach can be applied to model the N -junctions of perforates with more than one perforated pipe;
- For the case of zero mean flow, the Benson CPM approach is more accurate than the PLM one;
- For the case of non-zero mean flow, the Benson PLM approach gives some better results than the CPM one, but these results are not sufficient for judging the advantages and disadvantages of each case.

NOMENCLATURE

A_A entropy level

A^* starred form of dimensionless sound velocity
 C pressure loss coefficient
 F cross section
 h_o stagnation enthalpy
 k ratio of specific heats
 p pressure
 u gas velocity
 U^* starred form of dimensionless gas velocity
 ρ density
 λ_{in}^* starred (dimensionless) Riemann variable at the boundary

REFERENCES

1. Sapsford, S.M. "Application of non-linear modeling to intake and exhaust system design", *International Seminar High-Performance Spark Ignition Engines for Passenger Cars*, Technical Papers, Milano, Italy, November 5-6 (1992).
2. Onorati, A., Ferrari, G. and D'Errico, G. "The coupling of 1-D and 2-D fluid dynamic models for the prediction of unsteady flow in I.C. engine duct-systems", *IMEchE Int. Conf. Computational and Experimental Methods in Reciprocating Engines*, London, November 1-2 (2000).
3. Corberan, J.M. "A new constant pressure model for N -branch junctions", *Proc. Instn. Mech. Engrs, J. Auto. Engng*, **206**, pp 117-123 (1992).
4. Onorati, A. "Nonlinear fluid dynamic modeling of reactive silencers involving extended inlet/outlet and perforated ducts", *Noise Control Eng. J.*, **45**(1), (Jan/Feb 1997).
5. Onorati, A. "Numerical simulation of unsteady flows in I.C. engine silencers and the prediction of tailpipe noise", Chapter 6 in *Design Techniques for Engine Manifolds*, by D.E. Winterbone and R.J. Pearson, Professional Engineering Publishing, London (July 1999).
6. William-Louis, M.J.P., Ould-El-Hadrami, A. and Tournier, C. "On the calculation of unsteady compressible flow through an N -branch junction", *Proc. Instn. Mech. Engrs.*, **212**, part C, pp 49-56 (1998).
7. Winterbone, D.E. and Pearson, R.J. "Theory of engine manifold design (wave action methods for IC engine)", *Professional Eng. Pub.*, UK (2000).
8. Bingham, J.F. and Blair, G.P. "An improved branched pipe model for multi-cylinder automotive engine calculations", *Proc. Instn. Mech. Engrs.*, **199**(D1) (1985).
9. Bassett, M.D., Pearson, R.J. and Winterbone, D.E. "Steady-flow-coefficient estimation of exhaust manifold pulse-converter type junctions", SAE 1999-01-0213 (1999).

10. Morel, T., Morel, J. and Blaser, D.A. "Fluid dynamic and acoustic modeling of concentric-tube resonators/silencers", SAE 910072 (1991).
11. Benson, R.S. "The thermodynamics and gas dynamics of internal combustion engines", I, Clarendon Press, Oxford (1982).
12. Sullivan, J.W. "A method of modeling perforated tube muffler components. Part II applications", *J. Acoust. Soc. Am.*, **66**(3) (Sept. 1979).

APPENDIX

Entropy Level, Starred Variables and Continuity Equation

If the thermodynamic laws and ideal gas relations are combined, the following equation will be obtained.

$$\frac{p}{p_{\text{ref}}} = \left(\frac{a}{a_{\text{ref}}}\right)^{\frac{2k}{k-1}} e^{(-s+s_{\text{ref}})/R}. \quad (\text{A1})$$

Here, a and s are the sound speed and the entropy, respectively, and the subscript ref designated to the reference property. As shown in Figure A1, an isentropic process can be considered to occur from an arbitrary point (temperature T , pressure p and entropy s) to reference pressure (p_{ref}) line. By using Equation A1 for point A , the following relation will be resulted:

$$\left(\frac{a_A}{a_{\text{ref}}}\right)^{\frac{2k}{k-1}} = e^{(s_A - s_{\text{ref}})/R}. \quad (\text{A2})$$

If the normalized sound speed of point A is defined by $A_A \equiv \frac{a_A}{a_{\text{ref}}}$, Equation A3 will be obtained:

$$(A_A)^{\frac{2k}{k-1}} = e^{(s_A - s_{\text{ref}})/R}. \quad (\text{A3})$$

On the other hand, according to the isentropic process: $s_A = s$.

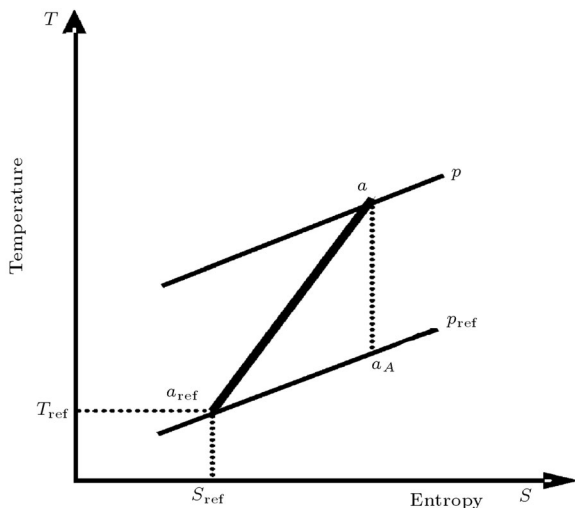


Figure A1. Entropy diagram.

Thus, relation $(A_A)^{\frac{2k}{k-1}} = e^{(s-s_{\text{ref}})/R}$ indicates the entropy level variation from arbitrary point (p, T) to Ref. point $(p_{\text{ref}}, T_{\text{ref}})$. Here, A_A is named entropy level. Equation A1 could be rearranged, such as the following equation, by using A_A for any non-homentropic flow:

$$\frac{p}{p_{\text{ref}}} = \left(\frac{a}{a_{\text{ref}}}\right)^{\frac{2k}{k-1}} \left(\frac{1}{A_A}\right)^{\frac{2k}{k-1}} = \left(\frac{A}{A_A}\right)^{\frac{2k}{k-1}}. \quad (\text{A4})$$

For homentropic flow $A_A = 1$.

The A , U and A_A are non-dimensional sound speed, flow velocity and entropy level, respectively. Also, the starred variables are defined as shown below, which are used to simplify equations:

$$U = \frac{u}{a_{\text{ref}}}, \quad U^* = \frac{U}{A_A},$$

$$A^* = \frac{A}{A_A}, \quad \lambda^* = \frac{\lambda}{A_A}. \quad (\text{A5})$$

By rearranging the continuity equation as follows:

$$\sum_j^N \rho_j U_j F_j = 0. \quad (\text{A6})$$

Density could be explained as shown below by combining the ideal gas relations and Equation A4:

$$\rho = \frac{p}{RT} = \frac{kp}{a^2} = k \left(\frac{p}{p_{\text{ref}}}\right) \left(\frac{a_{\text{ref}}^2}{a^2}\right) \left(\frac{p_{\text{ref}}}{a_{\text{ref}}^2}\right)$$

$$= k \left(\frac{A}{A_A}\right)^{\frac{2k}{k-1}} \left(\frac{1}{A^2}\right) \left(\frac{p_{\text{ref}}}{a_{\text{ref}}^2}\right)$$

$$= k A^* \frac{2k}{k-1} \left(\frac{1}{A^{*2} A_A^2}\right) \left(\frac{p_{\text{ref}}}{a_{\text{ref}}^2}\right). \quad (\text{A7})$$

By using the Riemann variable definition, the following equation can be obtained.

$$U = \frac{2}{k-1}(\lambda_{\text{in}} - A) = \frac{2}{k-1} A_A (\lambda_{\text{in}}^* - A^*). \quad (\text{A8})$$

Equations A7 and A8 can be replaced on Equation A5.

$$\sum_j^N (A_j^*)^{\frac{2k}{k-1}} \left(\frac{1}{A_{A_j}^2 A_j^{*2}}\right) A_{A_j} (\lambda_{\text{in}_j}^* - A_j^*) F_j$$

$$= \sum_j^N (A_j^*)^{\frac{2k}{k-1}} \left(\frac{\lambda_{\text{in}_j}^* - A_j^*}{A_{A_j}}\right) F_j = 0. \quad (\text{A9})$$

Pressure Loss Model Coefficients and Parameters

The experimental loss coefficients are written in Table A1 for six flow patterns of Figure 4. These coefficients are used to determine G_1 and G_2 functions, which were applied in Equation 13 and introduced in Table A2.

Table A1. Pressure loss coefficients of momentum equation of a streamline [11].

Flow Type	Pressure Drop	Coefficient
A	$p_1 - p_2 = C_1(\rho_2 u_2^2 - \rho_1 u_1^2)$	$C_1 = 0.3$
A	$p_1 - p_3 = C_2 \rho_3 u_3^2$	$C_2 = 0.6$
B	$p_3 - p_1 = C_3 \rho_1 u_1^2$	$C_3 = 0.75$
C	$p_2 - p_1 = C_4(\rho_1 u_1^2 - \rho_2 u_2^2)$	$C_4 = 0.9$
C	$p_3 - p_1 = C_5(\rho_1 u_1^2 - \rho_2 u_2^2)$	$C_5 = 0.9$
D	$p_1 - p_3 = C_6 \rho_3 u_3^2$	$C_6 = 0.85$

Acoustic Parameters

Some acoustic parameters have been in the main text which are described now. Transfer Function (TF) represents the sound attenuation in the system from the upstream to the downstream of it. The sound pressure level is the logarithmic effective pressure, such as:

$$\text{SPL} = 20 \log \frac{p_{\text{rms}} [N/m^2]}{2 \times 10^{-5} [N/m^2]} [\text{dB}], \quad (\text{A10})$$

and the transfer function:

$$\text{TF} = \text{SPL}_{\text{upstream}} - \text{SPL}_{\text{downstream}}. \quad (\text{A11})$$

Transmission Loss (TL) could be represented by the difference of upstream incident power and downstream transmitted power into an anechoic termination:

$$\text{TL} \equiv 10 \log \left| \frac{w_i}{w_t} \right|, \quad (\text{A12})$$

w_i and w_t can be obtained from the following Equations:

$$w_i = \frac{1}{2} \left[\left(\frac{1}{2} ((p_x)_{\text{rms}} + (\rho_o a_o u_x)_{\text{rms}}) \right)^2 F \right]_{\text{Upstream}}, \quad (\text{A13})$$

$$w_t = \frac{1}{2} \left[\left(\frac{1}{2} ((p_x)_{\text{rms}} + (\rho_o a_o u_x)_{\text{rms}}) \right)^2 F \right]_{\text{Downstream}}. \quad (\text{A14})$$

In the numerical methods used in this study, only the local magnitude of variables are known. Thus, the linear theory must be employed to obtain the incident and the transmitted parts of acoustic parameters. The following equation governs the acoustic perturbation theory:

$$\frac{\partial^2 p}{\partial t^2} = a_o \frac{\partial^2 p}{\partial x^2}. \quad (\text{A15})$$

The solution of it is:

$$p_x = A_+ e^{-ikx} + A_- e^{ikx}. \quad (\text{A16})$$

The first part of the solution is the incident part of pressure perturbation and the second one is the reflected part of it. Local velocity can be obtained similarly:

$$\rho_o a_o u_x = A_+ e^{-ikx} - A_- e^{ikx}. \quad (\text{A17})$$

By combining Equations A16 and A17, the following relation for calculating the incident part of pressure and velocity on the upstream will be obtained:

$$(p_x)_i = (\rho_o a_o u_x)_i = \frac{1}{2} (p_x + \rho_o a_o u_x). \quad (\text{A18})$$

Similarly, the transmitted part of pressure and velocity on the downstream with an anechoic condition will be resulted:

$$(p_x)_t = (\rho_o a_o u_x)_t = \frac{1}{2} (p_x + \rho_o a_o u_x). \quad (\text{A19})$$

Table A2. The functions G_1 and G_2 of pressure loss (Equation 13).

Flow Type	j	G_1	G_2	Flow Type	j	G_1	G_2
I	2	$C_1 k \left(\frac{U_2^*}{A_1^*} \right)^2$	$C_1 k \left(\frac{U_2^*}{A_1^*} \right)^2 + 1$	IV	2	$C_4 k \left(\frac{U_2^*}{A_1^*} \right)^2$	$C_4 k \left(\frac{U_1^*}{A_1^*} \right)^2 + 1$
	3	$C_2 k \left(\frac{U_3^*}{A_1^*} \right)^2$	1		3	0	$-C_5 k \left(\frac{U_2^*}{A_1^*} \right)^2 \left(\frac{A_2^*}{A_1^*} \right)^{\frac{2}{k-1}} + 1 + C_5 k \left(\frac{U_1^*}{A_1^*} \right)^2$
II	2	$C_1 k \left(\frac{U_2^*}{A_1^*} \right)^2$	$C_1 k \left(\frac{U_1^*}{A_1^*} \right)^2 + 1$	V	2	$C_4 k \left(\frac{U_2^*}{A_1^*} \right)^2$	$C_4 k \left(\frac{U_1^*}{A_1^*} \right)^2 + 1$
	3	$C_2 k \left(\frac{U_3^*}{A_1^*} \right)^2$	$\left(\frac{A_2^*}{A_1^*} \right)^{\frac{2k}{k-1}}$		3	0	1
III	2	$C_3 k \left(\frac{U_2^*}{A_1^*} \right)^2$	$C_3 k \left(\frac{U_1^*}{A_1^*} \right)^2 + 1$	VI	2	0	1
	3	0	$C_3 k \left(\frac{U_1^*}{A_1^*} \right)^2 + 1$		3	$C_6 k \left(\frac{U_3^*}{A_1^*} \right)^2$	1

Here, the $(p_x)_{\text{rms}}$ is the root mean square of local pressure and $(\rho_o a_o u_x)_{\text{rms}}$ is the root mean square of the product of the arbitrary density, the arbitrary sound speed and the local flow velocity.

Mean Flow

The tailpipe noise of the intake and exhaust system is caused by: (i) The pressure pulses and (ii) Mean

flow, which generates turbulence and vortex shedding at geometric discontinuities. It is possible to investigate the pulse noise and gas flow noise independently. Usually, the acoustic parameters of silencers are determined from their responses versus the reciprocating pulse noise with zero mean flow. The fluid flow velocity can be represented by mean and perturbation parts. When the mean flow velocity is zero, it is called zero mean flow.